Journal of Materials Chemistry A

Accepted Manuscript

ROYAL SOCIETY OF CHEMISTRY

www.rsc.org/materialsA

A-D-A-type *S*,*N*-Heteropentacene-based Hole Transport Materials for Dopant-free Perovskite Solar Cells

Christopher Steck,[a†] Marius Franckevičius,[bc†] Shaik Mohammed Zakeeruddin,[b*] Amaresh Mishra,[a*] Peter Bäuerle,[a] Michael Grätzel[b*]

[a]*Institute of Organic Chemistry II and Advanced Materials, University of Ulm, Albert-Einstein-Allee 11, 89081 Ulm, Germany. Email amaresh.mishra@uni-ulm.de*
[b]*Laboratory of Photonics and Interfaces, Institute of Chemical Sciences and Engineering, School of Basic Sciences, Ecole Polytechnique Fédérale de Lausanne (EPFL), CH-1015 Lausanne, Switzerland. Email: shaik.zakeer@epfl.ch, michael.graetzel@epfl.ch*
[c]*Center for Physical Sciences and Technology, Savanorių Ave. 231, LT-02300 Vilnius, Lithuania*.

[†]These authors contributed equally to this work.

Keywords: Heteroacene, Spectroscopy, Hole transport materials, Perovskite solar cell, Photo-induced absorption

Abstract

This work reports the design and synthesis of acceptor-donor-acceptor (A-D-A) type low band gap hole transport materials (HTM) comprising *S*,*N*-heteropentacene central units for solid-state perovskite-based solar cells. The optical and electrochemical properties were tuned by the insertion of thiophene or ethylenedioxythiophene units in the molecular backbone. These HTMs showed strong absorption in the visible region and suitable highest occupied molecular orbital (HOMO) and lowest unoccupied molecular orbital (LUMO) energies with respect to the $CH_3NH_3PbI_3$ perovskite. Mesoscopic solid state perovskite solar cells prepared by solution-

processing using these HTMs generated power conversion efficiencies (PCE) of 10.3-11.4% without the use of any additive or dopant. The charge transfer behavior between photoexcited perovskite and the HTMs was further investigated by photo-induced absorption spectroscopy.

Introduction

Recently, organometal halide $CH_3NH_3PbX_3$ (X = Cl, Br, I) perovskites[1, 2] have received considerable attention in solid-state photovoltaics due to their several interesting features, such as intense light absorption across the visible spectrum, high charge carrier mobilities, direct band gap, longer carrier diffusion length, and small exciton binding energy.[3-8] Miyasaka and co-workers were the first to report the incorporation of $CH_3NH_3PbX_3$ (X = Br, I) perovskite as sensitizer in liquid electrolyte-based dye-sensitized solar cells reaching power conversion efficiencies (PCE) of 3.8%.[9] Later, Park *et al*. reported efficient and stable solid-state $CH_3NH_3PbI_3$-based perovskite solar cells with PCEs as high as 9.7%.[3] Since then, by extensive optimization of the metal oxide scaffolds and device processing conditions PCEs have been improved to over 19% using state of the art 2,2',7,7'-tetrakis(*N*,*N*-di-*p*-methoxyphenylamino)-9,9'-spirobifluorene (spiro-MeOTAD) as hole transporting material.[10-12] Seok and co-workers reported a series of spiro-MeOTAD derivatives showing an enhanced PCE of 16.7% for the *o*-OMe substituted derivatives compared to the conventional p-OMe counterpart.[13] However, due to low hole mobility and conductivity of spiro-MeOTAD in the pristine form, additives, such as Lithium bis(trifluoromethanesulfonyl)imide (Li-TFSI)[14] and cobalt complexes as p-type dopants,[15] are necessary to improve the device performance. Although PCEs up to 12.8% were reported for HTM-free perovskite devices,[16-19] the most efficient solar cells usually employed organic HTMs which play a key role for the hole transport and reduce charge recombination processes.[20] In this respect, a wide range of material classes consisting of pyrene,[21] thiophene,[22,

[23] 3,4-ethylenedioxythiophene (EDOT),[24] butadine derivatives,[25, 26] carbazole,[27] star-shaped molecules,[28-30] tetrathiafulvalene,[31] triarylamines,[32] and poly(triarylamine)[11, 33, 34] have been developed as alternative organic HTMs showing excellent PCEs in the range from 10-15% by using various additives and dopants. All these HTMs have no absorption in the visible to near-infrared region, thus acting only as hole transporter while perovskite functions as light absorber. Several low band gap polymeric semiconductors have also been tested in perovskite devices showing PCEs in the range from 5-9%.[33, 35-38] Despite of having significant absorption in the visible region these polymers do not contribute to the photo-current and function only as hole conductor.

In order to reduce the process and optimization time and thereby the overall device cost, several dopant-free low band gap HTMs, such as star-shaped,[39] oligothiophene,[40] phenoxazine,[41] and phenothiazine[42] derivatives were developed showing excellent PCEs in the range of 12-13%. The star-shaped HTM containing quinolizino[3,4,5,6,7-*defg*]acridine core and oligothiophene branching units showed enhanced photocurrent in the blue region of the solar spectrum (400-600 nm).[39] We have recently employed dicyanovinyl (DCV)-capped acceptor-donor-acceptor (A-D-A) oligomers comprising dithieno[2,3-*d*:2',3'-*d*']thieno[3,2-*b*:4,5-*b*']dipyrroles (*S*,*N*-heteropentacene) as hole transport materials in $CH_3NH_3PbI_3$ perovskite devices exhibiting PCEs up to 10.5%.[43] Because of their strong absorption in the visible to near-infrared region, they also participate as light absorber together with perovskite in the low energy region. D-A-type sensitizers containing *S*,*N*-heteropentacene bridge and cyano acrylic acid anchoring group were currently used in dye-sensitized solar cells showing a moderate efficiency of 4-6%.[44] By using smaller DCV-substituted *S*,*N*-heteropentacenes higher PCEs of up to 6.5% were obtained in vacuum-processed and up to 4.9% in solution processed organic solar cells.[45, 46]

Acceptor-substituted *S,N*-heteroacenes combine the favourable properties of oligothiophenes, such as excellent stability due to a low lying HOMO energy level, and high charge carrier mobilities of oligoacenes.[47] In continuation to our work on the development of heteroacene-based HTMs, in this report we introduced thiophene and EDOT linkers between the planar *S,N*-heteropentacene central unit and DCV acceptor groups in A-D-A oligomers **1** and **2** and investigate the influence of the linker on optoelectronic and photovoltaic properties. In order to improve their solubility in organic solvents octylnonyl chains were introduced at the heteroacene nitrogens. In perovskite solar cells, fabricated by sequential solution-based deposition, high PCEs of 11.4% and 10.3% were achieved using **1** and **2** as dopant free HTMs in comparison with 7.1% for devices without hole transport layers. Due to their strong absorption in the visible and near-infrared region they also contribute to the charge transport and enhance the photocurrent of the device which can be seen in the incident photon to electron conversion efficiency (IPCE) spectra.

Results and Discussion

S,N-heteropentacene-based hole transport materials **1** and **2** were synthesized by Pd^0-catalyzed Stille cross-coupling reaction of bis-stannylated derivative **5** and DCV-substituted bromo-ethylenedioxythiophene **7** and bromothiophene **8** in yield of 70% and 60%, respectively (Scheme 1). Pd-catalyzed tandem Buchwald-Hartwig amination of 3,3',3",4'-tetrabromo-2,2':5',2"-terthiophene **3** with heptadecan-9-amine gave *S,N*-heteropentacene **4** in 50% yield. Bis-stannylation of **4** was carried out by lithiation using *n*-butyl lithium and subsequent quenching with trimethyltin chloride in 93% yield. 2-[(7-Bromo-2,3-dihydrothieno[3,4-*b*][1,4]dioxin-5-yl)methylene]malononitrile **7** was synthesized in 88% yield by a Knoevenagel condensation of 7-bromo-2,3-dihydrothieno[3,4-*b*][1,4]dioxine-5-carbaldehyde[48, 49] **6** and malononitrile in the presence of β-alanine as catalyst.

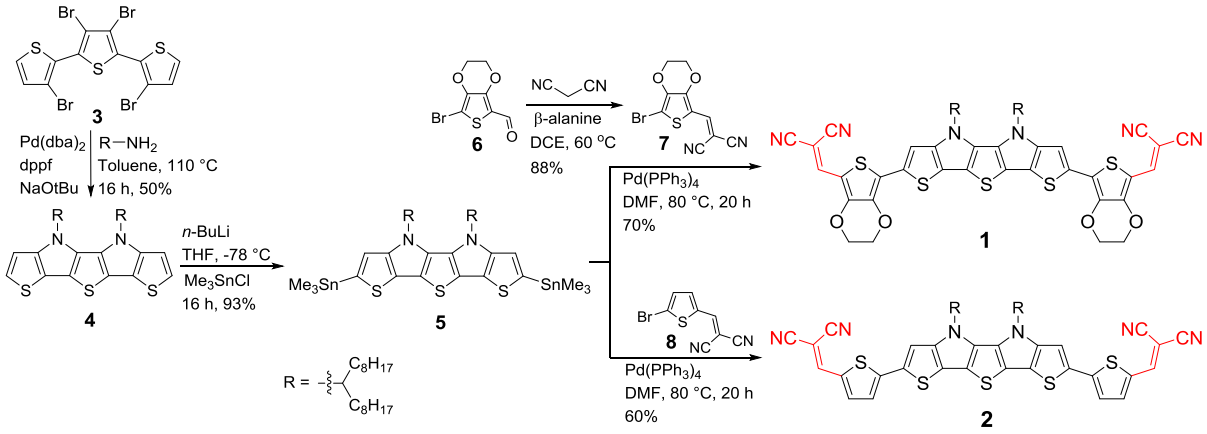

Scheme 1. Synthetic route of hole transport materials **1** and **2**.

The UV-Vis absorption profile of **1** and **2** in dichloromethane solution, coated on TiO_2 film and on top of perovskite layer are shown in Figure 1. All data are listed in Table 1. HTMs **1** and **2** showed strong intramolecular charge-transfer absorption bands at 683 and 655 nm, respectively, with high molar extinction coefficients (ε) of 137 500 M^{-1} cm^{-1} for **1** and 104 500 M^{-1} cm^{-1} for **2**. The red-shifted absorption ($\Delta\lambda = 28$ nm) and higher ε of HTM **1** can be ascribed to the more planar ground state geometry of the electron donating EDOT units caused by the lower degree of torsion due to S···O interactions. The strong absorption of the oligomers in the low energy region should serve the purpose of harvesting light transmitted through the perovskite layer.

In comparison to solution, a significant spectral broadening was observed for the absorption bands of **1** and **2** coated on TiO_2 surface. The absorption maximum of **1** was slightly blue-shifted (λ_{max} = 674 nm) compared to that measured in solution. On the other hand, the absorption band of **2** was strongly red-shifted and became structured (λ_{max} = 686 nm) indicating increased intermolecular interactions of the molecules in the solid state. The improved vibronic resolution on the absorption band of **2** might be arising from a better packing on the TiO_2 surface. It is interesting to note that, due to the absence of hexyl chain in the terminal thiophene

units the absorption band of HTM **2** is broadened and the onset is red-shifted by about 25 nm compared to the HTM **A** reported earlier (see ESI, Figure S1†).[43] This could be ascribed to improved packing of the molecule in the solid state. The optical energy gaps (E_g^{opt}) for **1** and **2** on TiO_2 film were 1.47 eV, which were lowered compared to the gaps (E_g = 1.63 eV for **1** and 1.68 eV for **2**) in solution. In order to further investigate the contribution of light absorption, thin films of HTM **1** and **2** coated on perovskite layer were investigated. The absorption of HTMs **1** and **2** on perovskite films further resembles the film spectra on TiO_2. As can be seen in Figure 2b, in the presence of HTMs the absorption band of perovskite films is strongly enhanced, specifically in the spectral region beyond 550 nm, further supporting the contribution of possible light absorption of the HTMs. Similar to the film spectra on TiO_2, the absorption band of HTM **2** on perovskite film is slightly structured and red-shifted compared to that of **1**. The enhanced absorption of these HTMs in the low energy region, exceeding up to 815 nm, could be beneficial for the overall photocurrent generation in the devices by absorbing the excess light that passes through the perovskite layer.

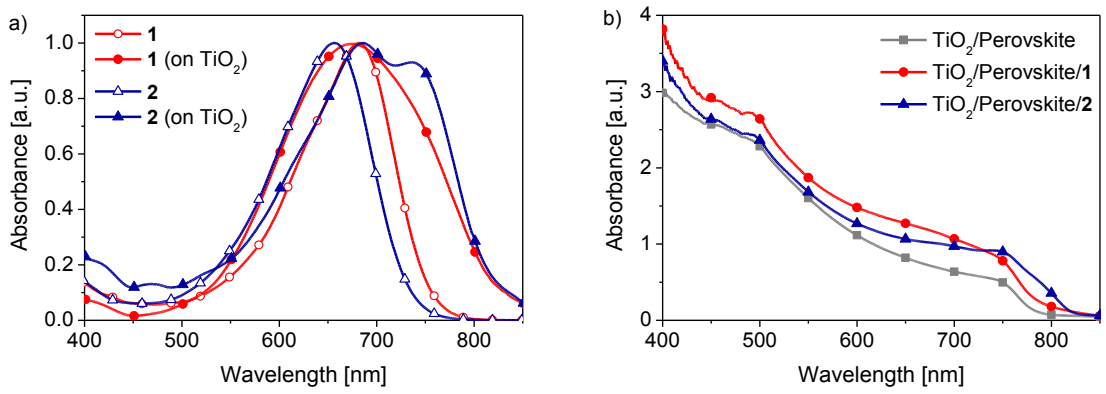

Figure 1. a) UV-Vis absorption spectra of HTMs **1** and **2** in dichloromethane solution and on TiO_2 film. b) Corresponding absorption spectra of TiO_2/perovskite films with and without HTMs.

Electrochemical measurement was performed in order to determine HOMO (highest occupied molecular orbital) and LUMO (lowest unoccupied molecular orbital) energy levels.

Figure 2 shows cyclic voltammograms of HTMs **1** and **2** and the data are summarized in Table 1. Two reversible oxidation processes were observed for both oligomers, which are assigned to the formation of stable radical cations and dications delocalized over the conjugated backbone. In the negative potential regime an irreversible reduction wave was observed indicating simultaneous radical anion formation on the terminal DCV groups. The insertion of EDOT units in oligomer **1** resulted in a slight negative shift of the oxidation potentials (ΔE_{ox} = 60 and 110 mV) compared to **2**. The HOMO and LUMO energy levels of oligomers **1** and **2** were determined from the onset of the first oxidation and reduction wave, respectively. The HOMO energy level of oligomer **1** is increased by 0.08 eV compared to **2**, while the LUMO energy level are similar at ~-3.8 eV. The trends are reflected in the energy level diagram and compares with the energy level of $CH_3NH_3PbI_3$ perovskite (Figure 3a). The LUMO energies of -3.8 eV allow sufficient offset to the conduction band minimum of perovskite to ensure efficient electron transfer at the interface.

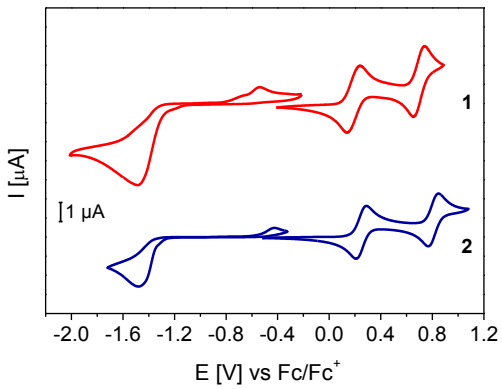

Figure 2. Cyclic voltammograms of HTM **1** and **2** measured in dichloromethane at 25 °C, supporting electrolyte $TBAPF_6$ (0.1 M), scan rate 100 mV s^{-1}.

The hole transport properties of oligomers **1** and **2** were determined from hole-only devices using the space charge limited current (SCLC) model. The extracted hole mobilities for **1** and **2** are 4.2 × 10^{-5} cm^2 V^{-1} s^{-1} and 3.5 × 10^{-5} cm^2 V^{-1} s^{-1}, respectively (see ESI, Fig. S2†).

Table 1. Optical and electrochemical properties of HTMs **1** and **2.**

HTM	λ_{abs} [nm] sol[a]	ε [M^{-1} cm^{-1}]	E_g^{opt} [eV] sol	λ_{abs} film [nm][b]	E_g^{opt} film [eV]	E^0_{ox1} [V][c]	E^0_{ox2} [V][c]	$E_{p\ red}$ [V][c]	HOMO [eV][d]	LUMO [eV][d]	E_g^{CV} [eV]
1	683	137 500	1.63	674	1.47	0.19	0.70	-1.49	-5.20	-3.80	1.40
2	655	104 500	1.68	686, 736	1.47	0.25	0.81	-1.48	-5.28	-3.77	1.51

[a]Absorption spectra were measured in dichloromethane. [b]Thin films were spin-coated on mp-TiO_2. [c]Cyclic voltammetry in dichloromethane/$TBAPF_6$ (0.1 M), scan rate = 100 mV/s, referenced against Fc/Fc^+. [d]HOMO/LUMO energy values were calculated by setting Fc/Fc^+_{vac} at -5.1 eV vs vacuum.

Figure 3b shows the schematic representation of the device architecture in which the $CH_3NH_3PbI_3$ perovskite layer was deposited on mesoporous-TiO_2 (mp-TiO_2) by two-step sequential deposition method as described in the experimental section. After annealing of the perovskite film, HTMs were deposited by spin-coating followed by deposition of a thin gold layer as back contact. As can be seen from the cross-section scanning electron microscopy (SEM) image in Figure 3c, the $CH_3NH_3PbI_3$ perovskite penetrate into the mp-TiO_2 and simultaneously forms an overlayer. Likewise, the HTMs infiltrate into the pores in TiO_2/perovskite layer and at the same time form a thin capping layer on the top.

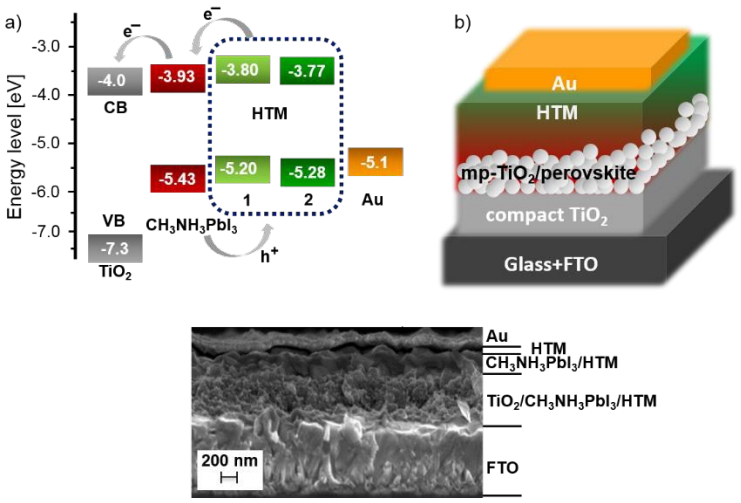

Figure 3. a) Schematic device architecture of investigated perovskite solar cells. b) Energy level diagram of the components used in solar cells described. c) Cross-sectional SEM image of a complete device.

Perovskite devices were fabricated using oligomers **1** and **2** as HTM and TiO_2 as electron transport layer. For comparison a reference device without HTM was also prepared. For the deposition of HTM layers different concentrations and film thicknesses have been tested. Current-voltage (*J*-*V*) characteristics of the devices are shown in Figure 4a and the photovoltaic parameters are summarized in Table 2. The best devices were obtained using HTM concentration of 0.03 M deposited at spin-speed of 2000 rpm. All photovoltaic data are listed in Table S1 (see ESI). The best performing device without any HTM displayed a short-circuit current density (J_{SC}) of 13.1 mA cm^{-2}, an open circuit voltage (V_{OC}) of 830 mV, and fill factor (FF) of 0.65, resulting in a PCE of 7.1%. The introduction of oligomers **1** and **2** as HTM significantly improved the PCE to 11.4% and 10.3%, respectively, and the FF attaining values up to 0.72, without the use of any additives and dopant. The resulting increase of the PCEs due to the presence of HTMs results from an improvement of all photovoltaic parameters, such as J_{SC}, V_{OC} and FF. The fill factor of devices based on HTM **1** and **2** were significantly improved (FF = >70%) compared to the device based on HTM **A** (FF = 65%) reported earlier.[43] This improvement could be ascribed to the better ordering of the molecule in the solid state. The average PCE values on a batch of five identical devices for HTM **1** and **2** are 11.24 ± 0.21% and 10.04±0.27%, respectively. The results clearly showed the crucial role of HTMs in perovskite devices. Perovskite devices fabricated with different HTM concentrations and spin speeds are presented in Table S1 (see ESI†). This improvement in device performance could be ascribed to the fact that the HTM layer acts as electron blocking layer and improves the charge extraction process. Thus the direct contact between the gold and perovskite is prevented to reduce non- radiative charge recombination.

The incident photon to electron conversion efficiency of perovskite devices with and without HTMs are presented in Figure 4b. As can be seen, the overall conversion efficiency

obtained with **1** and **2** is higher compared to the HTM-free device over the whole spectral range from 400-800 nm suggesting improved charge collection and extraction. In addition, HTMs **1** and **2** produce a red-shift in the IPCE spectra ($\Delta\lambda$ = 15-25 nm) which concurs with the absorption spectra of the films shown in Figure 1a. Although the IPCE spectra of HTM **2** device is red-shifted compared to HTM **1**, the lower IPCE in the spectral region from 400 to 650 nm for **1** yields a slightly lower J_{SC} values. The integrated current density from the IPCE spectra (16.14 mA cm^{-2} for **1**, 15.65 mA cm^{-2} for **2**, and 13.08 mA cm^{-2} for device without HTM) plotted in Fig. 4b is consistent with the value obtained from *J*–*V* curve. The results indicate that besides acting as HTM the low band gap molecules could also participate in the overall photocurrent generation.

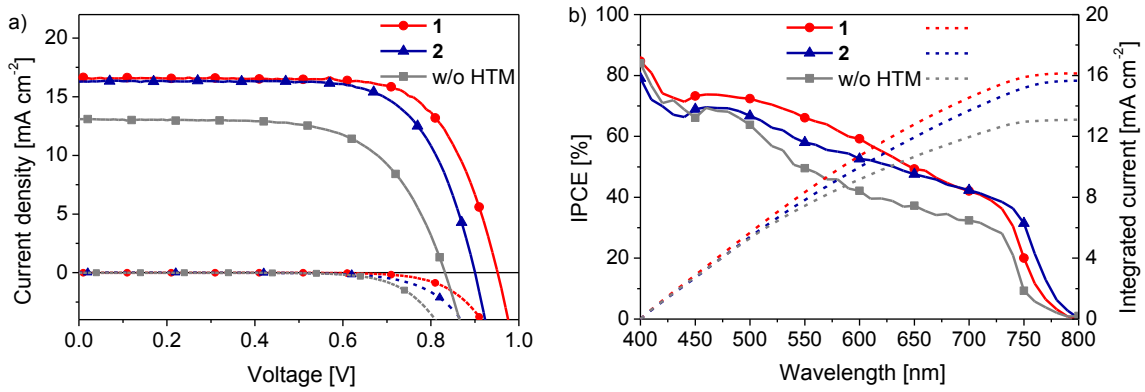

Figure 4. a) Current-voltage characteristics of the perovskite-based solar cell with HTMs **1** and **2** and the reference device without HTM measured in the dark and under 100 mW cm^{-2} photon flux (AM 1.5G) b) Corresponding IPCE spectra.

Table 2. Photovoltaic parameters of $CH_3NH_3PbI_3$-based solar cells with and without HTM.

HTM[a]	J_{SC} [mA cm^{-2}][b]	V_{OC} [mV][b]	FF[b]	PCE [%][b]
1	16.50 ± 0.12 (16.6)	951.4 ± 5.59 (953)	0.72 ± 0.005 (0.72)	11.24 ± 0.21 (11.4)
2	15.84 ± 0.71 (16.3)	899.6 ± 9.96 (899)	0.70 ± 0.009 (0.70)	10.04 ± 0.27 (10.3)
w/o HTM	13.1	832	0.65	7.1

[a][HTM] = 0.03 M and spin speed 2000 rpm. [b]Average data with standard deviation were based on five identical cells; the data for the best performing cells are given in parentheses. For device without HTM only the best data are included for comparison.

In order to further explain the light absorbing ability and photocurrent generation of the

HTMs we have fabricated devices with configuration of TiO_2/HTM **1** or **2**/Au without the perovskite layer. The devices showed very low J_{SC} and V_{OC} values (Fig. S3, Table S2, ESI†). The results indicated that both HTMs **1** and **2** could work as a light harvester and the charge separation occurs between TiO_2 and HTM. However, the lower performance is mainly due to the limitation of material loading and the possible fast charge recombination between TiO_2 and the HTM. These results further supports the contribution of the HTMs on the photocurrent generation together with the perovskite.

Further insight into the interfacial charge generation in the device was gained from photo-induced absorption (PIA) measurement on mp-TiO_2 film coated either with perovskite or the HTMs **1**, **2** or with both perovskite and HTM (Figure 5). The TiO_2/perovskite film showed an intense negative band at around 780 nm which can be attributed to the fluorescence of perovskite. Measurement of the TiO_2 film coated with HTM **1** in the absence of perovskite also showed a pronounced negative signal at around 850 nm in its fluorescence spectral range, while no absorption of the oxidized species could be observed in the near-infrared region. In the presence of perovskite a broad excited state absorption band appeared in the range from 1050-1400 nm with a maximum at 1190 nm assigned to the oxidized species of HTM **1**.

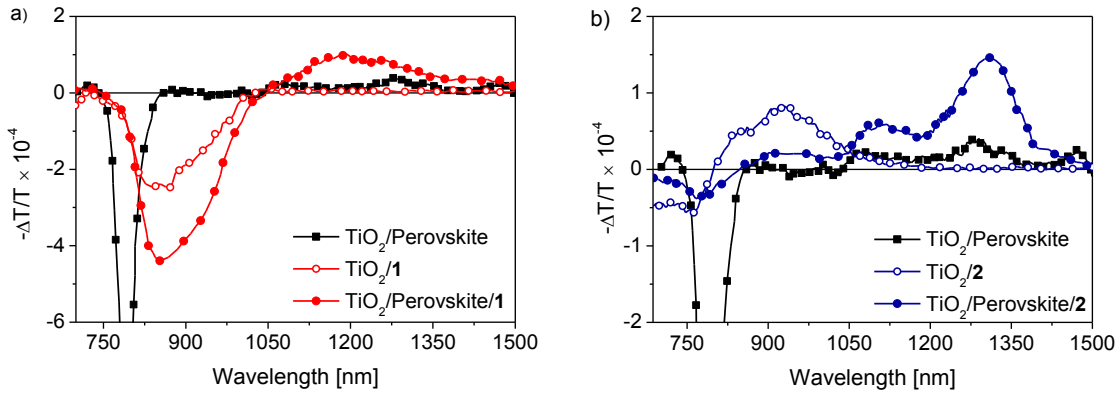

Figure 5. Photoinduced absorption (PIA) spectra of mp-TiO_2 films coated with perovskite, HTM **1**, and perovskite/**1** (a) and with perovskite, HTM **2**, and perovskite/**2** (b). Excitation wavelength λ_{ex} = 642 nm.

For HTM **2** coated on TiO_2, at shorter wavelengths a competition between negative and positive signals was revealed. The negative contribution below 850 nm is assigned to its fluorescence, while the positive signal at 930 nm can be attributed to the excited state absorption of the oxidized species. In the presence of perovskite the negative band attributed to the fluorescence of **2** is attenuated, while a new excited state absorption appears at longer wavelengths. The PIA results illustrate that efficient charge transfer takes place between the photoexcited perovskite and HTMs **1** and **2** under formation of long-lived charge carriers.

Conclusion

In summary, we have reported two new low band gap hole transporting materials **1** and **2** containing *S,N*-heteropentacene core flanked by EDOT/thiophene spacer and end-capped with dicyanovinylene acceptor units. The strong charge transfer absorption in the low energy region and suitable frontier orbital energy levels of the molecules allowed us to use them as HTM in $CH_3NH_3PbI_3$ perovskite solar cells. A strong red-shift was observed for both oligomers in thin films coated on TiO_2 as well as on perovskite. Specifically, oligomer **2** showed a structured absorption band in the low energy region which could be suitable for harnessing the extra light passing through the perovskite. Solar cells using HTMs **1** and **2** exhibited high FF up to 0.72 and PCEs of 11.4% and 10.3%, respectively. It is worth mentioning that the high performance of these devices was achievable even without the use of any additive and dopant. Additionally, the red-shifted IPCE spectra for the new HTMs in comparison to the devices without HTM further envisage the role of these HTMs in photocurrent generation together with the perovskite. Photoinduced absorption studies demonstrated occurrence of charge transfer between photoexcited HTM and perovskite. The present results offer a new avenue to fabricate high

efficiency and low cost perovskite solar cells by designing even more favourable hole transport materials with intense light absorption and tunable frontier orbital energy levels.

Experimental

Instrument and Measurements: NMR spectra were recorded on a Bruker DRX 400 spectrometer (^{1}H NMR: 400 MHz, ^{13}C NMR: 100 MHz). Chemical shift values (δ) are expressed in parts per million using residual solvent protons (^{1}H NMR: δ_H = 7.26 for $CDCl_3$; δ_H = 5.32 for CD_2Cl_2; ^{13}C NMR: δ_C = 77.0 for $CDCl_3$; δ_C = 54.0 for CD_2Cl_2) as internal standard. The splitting patterns are designated as follows: s (singlet), d (doublet), t (triplet) and m (multiplet). Elemental analyses were performed on an Elementar Vario EL. Melting points were determined using a Büchi Melting Point B-545. Thin layer chromatography was carried out on aluminum plates, pre-coated with silica gel, Merck Si60 F254. Preparative column chromatography was performed on glass columns packed with silica gel, Merck Silica 60, particle size 40−63 μm. High resolution MALDI-TOF mass spectra (HRMS) experiments were performed using a MS Bruker Reflex 2 (Bruker Daltonik GmbH, Bremen, Germany) using *trans*-2-[3-(4-*tert*-butyl-phenyl)-2-methyl-2-propenylidene]malononitrile (DCTB) as matrix. Cyclic voltammetry experiments were performed with a computer-controlled Autolab PGSTAT30 potentiostat in a three-electrode single-compartment cell with a platinum working electrode, a platinum wire counter electrode, and Ag/AgCl as reference electrode. All potentials were internally referenced to the ferrocene/ferrocenium couple.

Optical measurements: UV-Vis absorption spectra in dichloromethane solution were recorded on a Perkin Elmer Lambda 19 spectrometer. Optical absorption spectra of all investigated materials in thin films spin coated on the top of amorphous glass, TiO_2 and TiO_2/perovskite

were recorded with a CARY-5 UV-Vis-NIR spectrophotometer in transmission mode within the 500-850 nm range.

Mobility measurement. In order to assess the potential of HTMs **1** and **2** as hole transport materials, hole-only devices were fabricated using the space-charge-limited current (SCLC) method with the device structure ITO/PEDOT:PSS/HTM/Al. Hole mobilities were calculated using the Mott-Gurney law, by fitting Eq. 1 to experimental data in the voltage range where the obtained slope in the double log plot is equal to 2.

$$J = \frac{9}{8}\varepsilon_r \varepsilon_0 \mu_h \frac{V^2}{d^3} \qquad 1$$

In Equation 1, J is the current density, ε_0 is the permittivity of free space (8.85×10^{-12} F m^{-1}), ε_r is the relative permittivity of the material (approaching 3 for organic semiconductors), μ_h is the hole mobility, V is the applied voltage and d is the thickness of the active layer.

The hole-only devices were made by spin-coating PEDOT:PSS (Clevios P, VP Al4083) onto pre-cleaned, patterned indium tin oxide (ITO) substrates (15 Ω per square) (Kintec). A film of the HTM was spin-coated on top from chloroform solution with a concentration of 8 mg/mL. The film thickness was varied by using different spin-coating speeds. As counter electrode Al was deposited on top by vacuum evaporation. The current density–voltage curves of the devices were taken with a Keithley 2400 source.

Device fabrication: Devices were prepared on plasma-cleaned conductive fluorine-doped tin oxide (FTO) coated glass substrates. A compact 50 nm thick titanium dioxide layer was deposited by spray pyrolysis of 9 ml ethanol solution containing 0.6 mL titanium diisopropoxide bis(acetylacetonate) solution (75 wt% in 2-propanol, Sigma-Aldrich) and 0.4 mL acetylacetone at 450 °C in air. On top of this compact layer, a 350 nm-thick mesoporous titanium dioxide (TiO_2) layer was prepared by spin-coating 30 nm sized nanoparticles (Dyesol 30NRT,

Dyesol) diluted in ethanol (1:3.5 *wt*/*wt*) at 500 rpm for 20 s. The films were then gradually heated to 500 ^{o}C and sintered at that temperature for 1 h under oxygen atmosphere. Afterwards, lead iodide (PbI_2) was dissolved in *N*,*N*-dimethylformamide by vigorous stirring at 130 °C to obtain a 1.2 M stock solution. Led salt was spin coated on the top of mesoporous TiO_2 layer at 6500 rpm for 20 s and dried for 10 min at 85 ^{o}C. In order to assure better film coverage and pore filling, the deposition of PbI_2 was performed two times. Subsequently, on the top of the lead salt a 0.05 M CH_3NH_3I solution in ethanol was sprayed and left for 20 s before spin coating at 3000 rpm for 30 s. Formed perovskite films were dried at 85 ^{o}C for 15 min. Subsequently, for devices with hole transporting materials, compounds **1** and **2** were dissolved in tetrachloro-ethane (0.03 M) and deposited on top of the perovskite layer by spin coating at 2000 rpm for 20 s while keeping solutions at 70 ^{o}C degrees during the whole procedure. Device fabrication was completed by thermal evaporation of 60 nm thick gold layer on top of the pure perovskite and perovskite with HTM. The active area of the devices is approx. 0.56 cm^2

J-V Characterization: The *J-V* characteristics of the devices were measured under 100mW/cm^2 conditions using a 450 W Xenon lamp (Oriel) as a light source, equipped with a Schott K113 Tempax sunlight filter (Präzisions Glas & Optik GmbH) to match the emission spectra to the AM1.5G standard in the region of 350-750 nm. The current–voltage characteristics of the devices were obtained by applying external potential bias to the cell while recording the generated photocurrent using a Keithley (Model 2400) digital source meter. The *J–V* curves of all devices were measured by masking the active area with a metal mask of 0.16 cm^2. The internal photon to current conversion efficiency (IPCE) of the devices was measured by focusing light from a 300 W Xenon lamp (ILC Technology, U.S.A.) through a Gemini-180 double monochromator (Jobin Yvon Ltd., U.K.) while chopping at 3 Hz before illuminating onto the photovoltaic cell. The monochromator was incremented through the visible spectrum

to generate the IPCE dependence on wavelength. Photoinduced absorption (PIA) spectroscopy of the films was measured using home implemented setup as described earlier.[50]

4,5-Bis(1-octylnonyl)-dithieno[2,3-*d*:2'3'-*d*]thieno[3,2-*b*:4,5-*b*']dipyrrole (4). A solution of 3,3',3",4'-tetrabromo-2,2':5',2"-terthiophene **3** (1.00 g, 1.78 mmol), $Pd(dba)_2$ (0.10 g, 0.17 mmol), dppf (0.40 g, 0.73 mmol) and sodium *tert.* butoxide (2.94 g, 30.57 mmol) in 24 mL dry toluene was stirred at r.t. for 30 min. Then heptadecan-9-amine (1.22 g, 4.76 mmol) was added and the reaction mixture was heated at 110°C for 16 h. After the reaction mixture was cooled to r.t., deionised water was added and the reaction mixture was extracted with DCM. The combined organic layers were dried with $MgSO_4$ and the solvent was removed under reduced pressure. The brown oil was purified by column chromatography (silica, petrol ether) to isolate the product **4** (0.67 g, 0.89 mmol, 50%) as slightly yellow solid. Mp.: 57-59 °C. ^{1}H NMR (400 MHz,CD_2Cl_2): δ [ppm] = 7.14 (d, ^3J = 5.3 Hz, 2H, α-Th), 7.08 (d, ^3J = 5.3 Hz, 2H, β-Th), 4.69-4.62 (m, 2H, N-CH), 2.11-2.02 (m, 4H, CH_2), 1.98-1.90 (m, 4H, CH_2), 1.37-1.28 (m, 48H, CH_2), 0.83 (t, ^3J = 6.9 Hz, 12H, CH_3). ^{13}C NMR (100 MHz, CD_2Cl_2): δ [ppm] = 142.04, 133.49, 130.96, 121.91, 119.36, 115.76, 114.50, 62.02, 35.76, 32.40, 30.24, 29.97, 29.76, 27.18, 23.22, 14.41 HRMS (MALDI-TOF): *m/z* [M^+] = 750.50031 (calc. for $C_{46}H_{74}N_2S_3$: 750.50086) (δm/m = 0.7 ppm).

2,7-Bis(trimethylstannyl)4,5-bis(1-octylnonyl)-dithieno[2,3-*d*:2'3'-*d*]thieno[3,2-*b*:4,5-*b*']dipyrrole (5). 4,5-Bis(1-octylnonyl)-dithieno[2,3-*d*:2'3'-*d*]thieno[3,2-*b*:4,5-*b*']dipyrrole **4** (212.2 mg, 0.28 mmol) was dissolved in 5 mL dry THF and cooled to -78 °C. A 1.6 M solution of *n*-BuLi in hexane (0.56 mL, 0.73 mmol) was added drop wise and the reaction mixture was stirred for additional 1 h. $SnMe_3Cl$ (168.0 mg, 0.84 mmol) dissolved in 1 mL dry THF was added and the reaction mixture was stirred in the cooling bath for 30 min and 5 h at r.t. The reaction was quenched by adding deionised water. The layers were separated and the aqueous

layer was extracted with DEE (2x20 mL). The combined organic layers were dried over $MgSO_4$. The solvent was removed to yield **5** as dark yellow oil (284.5 mg, 0.26 mmol) in 93% yield. The product was used without further purification. ^{1}H NMR (400 MHz, CD_2Cl_2): δ [ppm] = 7.12 (s, 2H, T-H), 4.63 (m, 2H, CH), 2.09-2.04 (m, 4H, CH^2), 1.96-1.91 (m, 4H, CH_2), 1.26-1.18 (m, 48H, CH_2), 0.83 (t, ^3J = 6.8Hz, 12H, CH_3), 0.41 (s, 18H, Sn-CH_3). ^{13}C NMR (100 MHz, CD_2Cl_2): δ [ppm] = 144.82, 134.89, 133.69, 121.26, 61.87, 35.67, 32.52, 32.40, 30.28, 30.18, 29.95, 29.77, 27.18, 23.22, 14.43, 7.88. HRMS (MALDI-TOF): *m/z* [M^+] = 1078.43121 (calc. for $C_{52}H_{90}N_2S_3Sn_2$: 1078.43101) (δm/m = 0.2 ppm).

2-[(7-Bromo-2,3-dihydrothieno[3,4-*b*][1,4]dioxin-5-yl)methylene]malononitrile (7). 7-Bromo-2,3-dihydrothieno[3,4-*b*][1,4]dioxine-5-carbaldehyde **6** (308.8 mg, 1.24 mmol), malononitrile (1.715 g, 25.96 mmol) and β-alanine (5.52 mg, 0.06 mmol) were dissolved in 3 mL DCE. The reaction mixture was heated at 60 °C for 2 d. Deionized water and DCM were added and the layers were separated. The combined organic layer was washed thoroughly with water to remove the excess of malononitrile. The solvent was removed to yield a brown solid. After column chromatography product **7** was obtained as yellow solid (323.3 mg, 1.09 mmol) in 88% yield. Mp.: 172-173 °C. ^{1}H NMR (400 MHz, $CDCl_3$): δ [ppm] = 7.83 (s, 1H, $HC=C(CN)_2$), 4.34 – 4.41 (m, 4H, -O-CH_2-). ^{13}C NMR (100 MHz, $CDCl_3$): δ [ppm] = 148.03, 145.35, 140.56, 114.63, 113.94, 112.82, 104.05, 73.67, 65.95, 64.95.MS (CI): *m/z* [M^+] = 297. Elemental analysis: calc. (%) for $C_{10}H_5BrN_2O_2S$: C 40.42, H 1.70, N 9.43, S 10.79; found: C 40.60, H 2.03, N 9.77, S 11.07.

2,2'-[4,5-Bis(1-octylnonyl)-dithieno[2,3-*d*:2'3'-*d*]thieno[3,2-*b*:4,5-*b*']dipyrrole-2,7-diyl)-bis(2,3-dihydrothieno[3,4-*b*][1,4]dioxin-5,5'-diyl)bis(methane-1-yl-1-ylidine)]dimalononitrile (1). 2-((7-Bromo-2,3-dihydrothieno[3,4-*b*][1,4]dioxin-5-yl)methylene)malononitrile **7** (187.0 mg, 0.63 mmol) and 2,7-bis(trimethylstannyl)4,5-bis(1-octylnonyl)-dithieno[2,3-d:2'3'-

dthieno[3,2-*b*:4,5-*b*']dipyrrole **5** (284.5 mg, 0.26 mmol) were dissolved in 5 mL of dry DMF. The reaction mixture was purged with argon for 15 min, then $Pd(PPh_3)_4$ (19.1 mg, 0.02 mmol) was added. The reaction was heated to 80 °C for 20 h. After removing the solvent in vaccuo, the crude product was purified by column chromatography (flash silica, DCM) to yield the product **1** (219.9 mg, 0.19 mmol, 70%) as dark blue solid with a golden gloss. Mp.: 264.3 °C. ^{1}H NMR (400 MHz, CD_2Cl_2): δ [ppm] = 7.81 (s, 2H, H-DCV), 7.53 (s, 2H, H-SN5), 4.70-4.62 (m, 2H, CH), 4.49 (s, 8H, O-CH_2-), 2.16-1.97 (m, 8H; CH2), 1.32-1.05 (m, 48H, CH2), 0.81 (t, ^3J = 6.8 Hz, 12 H, CH_3). ^{13}C NMR (100 MHz, CD_2Cl_2): δ [ppm] = 149.85, 144.19, 134.65, 123.60, 116.56, 115.73, 113.42, 109.59, 66.56, 65.56, 62.59, 35.63, 32.37, 30.14, 30.01, 29.74, 27.37, 23.18, 14.39. HRMS (MALDI-TOF): *m/z* [M^+] = 1182.49939 (calc. for $C_{66}H_{82}N_6O_4S_5$: 1182.49956) (δm/m = 0.1 ppm).

2,2'-[4,5-Bis(1-octylnonyl)-dithieno[2,3-*d*:2'3'-*d*]thieno[3,2-*b*:4,5-*b*']dipyrrole-2,7-diyl)bis-(thien-5,5'-diyl)bis(methane-1-yl-1-ylidine)]dimalononitrile (2). 2-((5-Bromothiophen-2-yl)methylene)malononitrile **8** (168.0 mg, 0.70 mmol) and 2,7-bis(trimethylstannyl)4,5-bis(1-octylnonyl)-dithieno[2,3-d:2'3'-d]thieno[3,2-*b*:4,5-*b*']dipyrrole **5** (288.0 mg, 0.27 mmol) were dissolved in 5 mL abs. DMF. The reaction mixture was purged with argon for 15 min, then $Pd(PPh_3)_4$ (19.2 mg, 0.02 mmol) was added. The reaction was heated to 80 °C for 20 h. After removing the solvent *in vaccuo*, the crude product was purified by column chromatography (flash silica, DCM) to yield the product **2** (171.2 mg, 0.16 mmol, 60%) as dark blue solid. Mp.: 265.8 °C. ^{1}H NMR (400 MHz, CD_2Cl_2): δ [ppm] = 7.72 (s, 2H, H-DCV), 7.62 (d, ^3J = 4.2 Hz, 2H, Th β-H), 7.48 (s, 2H, β-H SN5), 7.30 (d, ^3J = 4.2 Hz, 2H, Th β-H), 4.70-4.62 (m, 2H, CH), 2.15-1.97 (m, 8H, CH_2), 1.27-1.05 (m, 48 H, CH_2), 0.81 (t, ^3J = 6.6 Hz, 12 H, CH_3). ^{13}C NMR (100 MHz, CD_2Cl_2): δ [ppm] = 151.48, 150.34, 143.12, 141.54, 134.69, 133.25, 132.35, 124.11, 122.51, 118.50, 115.37, 114.62, 114.62, 113.72, 74.66, 62.67, 35.64, 32.35, 30.05, 29.94, 29.69,

27.21, 23.18, 14.38. HRMS (MALDI-TOF): *m/z* [M^+] = 1066.48505 (calc. for $C_{62}H_{78}N_6S_5$: 1066.48860) (δm/m = 3.3 ppm).

Acknowledgments

This work was supported by the German Ministry for Education and Research (BMBF, program LOTsE 03EK3505G). M.G. thanks the Swiss Confederation for funding under the Sciex-NMS exchange program (Project Code 13.194) and CCEM-CH in the 9th call proposal 906: CONNECT PV. The authors also thankful to Jingshan Luo for SEM measurements.

References

1. K. Liang, David B. Mitzi and M. T. Prikas, *Chem. Mater.*, 1998, **10**, 403–411.
2. D. B. Mitzi, *J. Mater. Chem. A*, 2004, **14**, 2355-2365.
3. H.-S. Kim, C.-R. Lee, J.-H. Im, K.-B. Lee, T. Moehl, A. Marchioro, S.-J. Moon, R. Humphry-Baker, J.-H. Yum, J. E. Moser, M. Grätzel and N.-G. Park, *Sci. Rep.*, 2012, **2**, 591 doi:510.1038/srep00591.
4. M. M. Lee, J. Teuscher, T. Miyasaka, T. N. Murakami and H. J. Snaith, *Science*, 2012, **338**, 643-647.
5. J. Burschka, N. Pellet, S.-J. Moon, R. Humphry-Baker, P. Gao, M. K. Nazeeruddin and M. Grätzel, *Nature*, 2013, **499**, 316–319.
6. M. Liu, M. B. Johnston and H. J. Snaith, *Nature*, 2013, **501**, 395–398.
7. N.-G. Park, *Mater. Today*, 2014, **18**, 65–72.
8. S. P. Singh and P. Nagarjuna, *Dalton Trans.*, 2014, **43**, 5247-5251.
9. A. Kojima, K. Teshima, Y. Shirai and T. Miyasaka, *J. Am. Chem. Soc.*, 2009, **131**, 6050-6051.
10. H. Zhou, Q. Chen, G. Li, S. Luo, T.-b. Song, H.-S. Duan, Z. Hong, J. You, Y. Liu and Y. Yang, *Science*, 2014, **345**, 542-546.
11. N. J. Jeon, J. H. Noh, Y. C. Kim, W. S. Yang, S. Ryu and S. I. Seok, *Nat. Mater.*, 2014, **13**, 897–903.
12. N. J. Jeon, J. H. Noh, W. S. Yang, Y. C. Kim, S. Ryu, J. Seo and S. I. Seok, *Nature*, 2015, **517**, 476-480.
13. N. J. Jeon, H. G. Lee, Y. C. Kim, J. Seo, J. H. Noh, J. Lee and S. I. Seok, *J. Am. Chem. Soc.*, 2014, **136**, 7837–7840.
14. H. J. Snaith and M. Grätzel, *Appl. Phys. Lett.*, 2006, **89**, 262114(262111)-262114(262113).
15. J. Burschka, A. Dualeh, F. Kessler, E. Baranoff, N.-L. Cevey-Ha, C. Yi, M. K. Nazeeruddin and M. Grätzel, *J. Am. Chem. Soc.*, 2011, **133**, 18042–18045.
16. L. Etgar, P. Gao, Z. Xue, Q. Peng, A. K. Chandiran, B. Liu, M. K. Nazeeruddin and M. Grätzel, *J. Am. Chem. Soc.*, 2012, **134**, 17396–17399.
17. F. Hao, C. C. Stoumpos, Z. Liu, R. P. H. Chang and M. G. Kanatzidis, *J. Am. Chem. Soc.*, 2014, **136**, 16411–16419.
18. J. Shi, J. Dong, S. Lv, Y. Xu, L. Zhu, J. Xiao, X. Xu, H. Wu, D. Li, Y. Luo and Q. Meng, *Appl. Phys. Lett.*, 2014, **104**, 063901.
19. A. Mei, X. Li, L. Liu, Z. Ku, T. Liu, Y. Rong, M. Xu, M. Hu, J. Chen, Y. Yang, M. Grätzel and H. Han, *Science*, 2014, **345**, 295-298.
20. T. Swetha and S. P. Singh, *J. Mater. Chem. A*, 2015, DOI: 10.1039/C1035TA02507A.
21. N. J. Jeon, J. Lee, J. H. Noh, M. K. Nazeeruddin, M. Grätzel and S. I. Seok, *J. Am. Chem. Soc.*, 2013, **135**, 19087–19090.
22. H. Li, K. Fu, P. P. Boix, L. H. Wong, A. Hagfeldt, M. Grätzel, S. G. Mhaisalkar and A. C. Grimsdale, *ChemSusChem*, 2014, **7**, 3420–3425.

23. K. Thirumal, K. Fu, P. P. Boix, H. Li, T. M. Koh, W. Leong, S. Powar, A. C. Grimsdale, M. Gratzel, N. Mathews and S. G. Mhaisalkar, *J. Mater. Chem. A*, 2014, **2**, 6305-6309.
24. H. Li, K. Fu, A. Hagfeldt, M. Grätzel, S. G. Mhaisalkar and A. C. Grimsdale, *Angew. Chem. Int. Ed.*, 2014, **53**, 4085–4088.
25. S. Lv, L. Han, J. Xiao, L. Zhu, J. Shi, H. Wei, Y. Xu, J. Dong, X. Xu, D. Li, S. Wang, Y. Luo, Q. Meng and X. Li, *Chem. Commun.*, 2014, **50**, 6931-6934.
26. J. Xiao, L. Han, L. Zhu, S. Lv, J. Shi, H. Wei, Y. Xu, J. Dong, X. Xu, Y. Xiao, D. Li, S. Wang, Y. Luo, X. Li and Q. Meng, *RSC Adv.*, 2014, **4**, 32918-32923.
27. B. Xu, E. Sheibani, P. Liu, J. Zhang, H. Tian, N. Vlachopoulos, G. Boschloo, L. Kloo, A. Hagfeldt and L. Sun, *Adv. Mater.*, 2014, **26**, 6629–6634.
28. K. Do, H. Choi, K. Lim, H. Jo, J. W. Cho, M. K. Nazeeruddin and J. Ko, *Chem. Commun.*, 2014, **50**, 10971-10974.
29. H. Choi, S. Paek, N. Lim, Y. Lee, M. K. Nazeeruddin and J. Ko, *Chem.–Eur. J.*, 2014, **20**, 10894–10899.
30. H. Choi, S. Park, S. Paek, P. Ekanayake, M. K. Nazeeruddin and J. Ko, *J. Mater. Chem. A*, 2014, **2**, 19136-19140.
31. J. Liu, W. Yongzhen, C. Qin, X. Yang, T. Yasuda, A. Islam, K. Zhang, W. Peng, W. Chen and L. Han, *Energy Environ. Sci.*, 2014, **7**, 2963-2967.
32. L. E. Polander, P. Pahner, M. Schwarze, M. Saalfrank, C. Koerner and K. Leo, *APL Mat.*, 2014, **2**, 081503.
33. J. H. Heo, S. H. Im, J. H. Noh, T. N. Mandal, C.-S. Lim, J. A. Chang, Y. H. Lee, H.-j. Kim, A. Sarkar, M. K. Nazeeruddin, M. Grätzel and S. I. Seok, *Nat. Photon.*, 2013, **7**, 486–491.
34. D. Bi, G. Boschloo and A. Hagfeldt, *Nano*, 2014, **09**, 1440001.
35. W. Zhang, B. Cai, Y. Xing, Z. Yang and J. Qiu, *Energy Environ. Sci.*, 2013, **6**, 1480-1485.
36. Y. S. Kwon, J. Lim, H.-J. Yun, Y.-H. Kim and T. Park, *Energy Environ. Sci.*, 2014, **7**, 1454-1460.
37. A. Abrusci, S. D. Stranks, P. Docampo, H.-L. Yip, A. K.-Y. Jen and H. J. Snaith, *Nano Lett.*, 2013, **3**, 3124–3128.
38. P. Nagarjuna, K. Narayanaswamy, T. Swetha, G. H. Rao, S. P. Singh and G. D. Sharma, *Electrochim. Acta*, 2015, **151**, 21-26.
39. P. Qin, S. Paek, M. I. Dar, N. Pellet, J. Ko, M. Grätzel and M. K. Nazeeruddin, *J. Am. Chem. Soc.*, 2014, **136**, 8516–8519.
40. L. Zheng, Y.-H. Chung, Y. Ma, L. Zhang, L. Xiao, Z. Chen, S. Wang, B. Qu and Q. Gong, *Chem. Commun.*, 2014, **50**, 11196-11199.
41. M. Cheng, B. Xu, C. Chen, X. Yang, F. Zhang, Q. Tan, Y. Hua, L. Kloo and L. Sun, *Adv. Energy Mater.*, 2015, 1401720.
42. M. Cheng, C. Chen, X. Yang, J. Huang, F. Zhang, B. Xu and L. Sun, *Chem. Mater.*, 2015, **27**, 1808–1814.
43. P. Qin, H. Kast, M. K. Nazeeruddin, S. M. Zakeeruddin, A. Mishra, P. Bäuerle and M. Grätzel, *Energy Environ. Sci.*, 2014, **7**, 2981-2985.
44. Z. Wang, M. Liang, Y. Tan, L. Ouyang, Z. Sun and S. Xue, *J. Mater. Chem. A*, 2015, **3**, 4865-4874.
45. A. Mishra, D. Popovic, A. Vogt, H. Kast, T. Leitner, K. Walzer, M. Pfeiffer, E. Mena-Osteritz and P. Bäuerle, *Adv. Mater.*, 2014, **26**, 7217–7223.
46. H. Kast, A. Mishra, G. L. Schulz, M. Urdanpilleta, E. Mena-Osteritz and P. Bäuerle, *Adv. Funct. Mater.*, 2015, **25**, 3414–3424.
47. C. Wetzel, A. Mishra, E. Mena-Osteritz, A. Liess, M. Stolte, F. Würthner and P. Bäuerle, *Org. Lett.*, 2014, **16**, 362–365.
48. H. Jian and J. M. Tour, *J. Org. Chem.*, 2005, **70**, 3396-3424.
49. M. Jessing, M. Brandt, K. J. Jensen, J. B. Christensen and U. Boas, *J. Org. Chem.*, 2006, **71**, 6734-6741.
50. S. Mathew, A. Yella, P. Gao, R. Humphry-Baker, B. F. E. Curchod, N. Ashari-Astani, I. Tavernelli, U. Rothlisberger, M. K. Nazeeruddin and M. Grätzel, *Nat. Chem.*, 2014, **6**, 242–247.

Table of Content

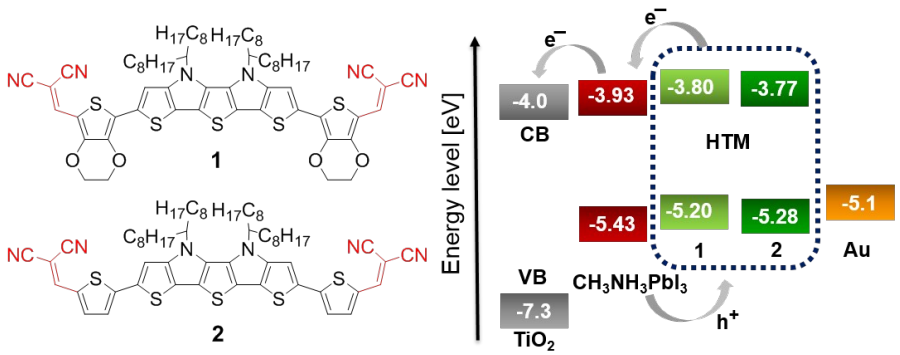

Heteropentacene-based A-D-A type hole transport materials with suitable frontier orbital energy levels were synthesized and implemented in perovskite-based solar cells generating promising power conversion efficiencies up to 11.4%.

Table of Content

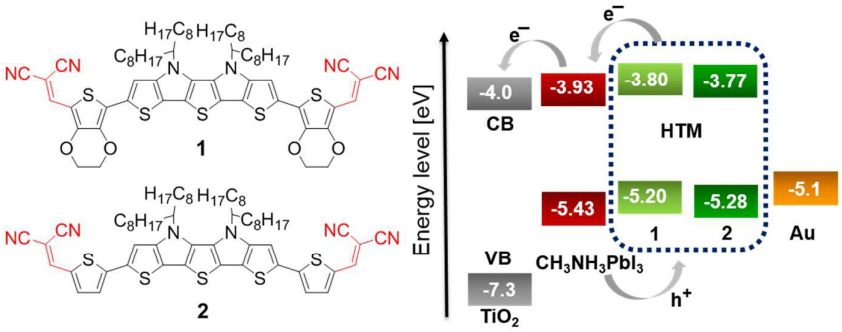

Heteropentacene-based A-D-A type hole transport materials with suitable frontier orbital energy levels were synthesized and implemented in perovskite-based solar cells generating promising power conversion efficiencies up to 11.4%.